THE JOURNAL OF PHYSICAL CHEMISTRY C

Article

pubs.acs.org/JPCC

Electronic Polarization at Pentacene/Polymer Dielectric Interfaces: Imaging Surface Potentials and Contact Potential Differences as a Function of Substrate Type, Growth Temperature, and Pentacene Microstructure

Yanfei Wu,[†] Greg Haugstad,[‡] and C. Daniel Frisbie*,[†]

[†]Department of Chemical Engineering and Materials Science, and [‡]Characterization Facility, University of Minnesota, Minneapolis, Minnesota 55455, United States

Supporting Information

ABSTRACT: Interfaces between organic semiconductors and dielectrics may exhibit interfacial electronic polarization, which is equivalently quantified as a contact potential difference (CPD), an interface dipole, or a vacuum level shift. Here we report quantitative measurements by scanning Kelvin probe microscopy (SKPM) of surface potentials and CPDs across ultrathin (1−2 monolayer) crystalline islands of the benchmark semiconductor pentacene thermally deposited on a variety of polymer dielectrics (e.g., poly(methyl methacrylate), polystyrene). The CPDs between the pentacene islands and the polymer substrates are in the range of −10 to +50 mV, they depend strongly on the polymer type and deposition temperature, and the CPD magnitude is correlated with the dipole moment of the characteristic monomers. Surface potential variations within 2 monolayer (3 nm) thick pentacene islands are ∼15 mV and may be ascribed to microstructure (epitaxial) differences. Overall, the microscopy results reveal both strong variations in interfacial polarization and lateral electrostatic heterogeneity; these factors ultimately should affect the performance of these interfaces in devices.

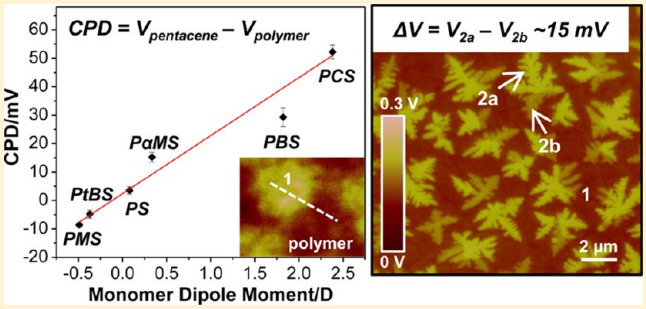

INTRODUCTION

It is well-known from photoelectron spectroscopy that interfaces between organic semiconductors and metals (O/M interfaces) or between two organic semiconductors (O/O interfaces) can exhibit significant polarization, i.e., a vacuum level shift, or contact potential difference (CPD) may be present at the interface.[1−9] Interfacial polarization, which may be due to interface dipoles or charge transfer,[3,5,10,11] is important because the resulting electric fields exert a strong influence on electronic structure and energy level alignment (i.e., the semiconductor density of states, DOS). For example, interface dipoles can cause a shift of the highest occupied molecular orbital manifold (HOMO band) compared to the organic semiconductor bulk, and such shifts or "band-bending" are critical to the electrical performance of O/M and O/O interfaces in devices such as solar cells,[12−14] light-emitting diodes,[15,16] and transistors.[17]

Interfaces between organic semiconductors and insulators (O/I interfaces), on the other hand, are also important for devices, particularly organic field effect transistors (OFETs),[18−23] but they are more challenging to investigate by photoelectron spectroscopy because of electrostatic charging. Consequently, less is known about O/I CPDs, although this knowledge is important for obtaining a better microscopic picture of charge transport in OFETs.

Scanning Kelvin probe microscopy (SKPM) offers an attractive alternative to photoelectron spectroscopy for recording vacuum level shifts and CPDs at O/I interfaces.[24−30] In SKPM, surface potentials (work functions) are recorded and mapped; differences in surface potentials between two materials in contact with each other (e.g., a patchy film on a substrate) give the CPD. Significantly, SKPM is not as susceptible to electrostatic charging as it does not rely on electron photoemission but rather on capacitive coupling between a sharp probe and the sample.[28,31] This makes SKPM readily applicable to O/I interfaces. In addition, high resolution surface potential maps by SKPM can be correlated directly with simultaneously recorded topographic images, which allows assessment of how subtle microstructural features impact the interfacial electrostatics. Surprisingly, relatively little work has been reported in the literature concerning application of SKPM (or a related technique, electrostatic force microscopy) to organic interfaces, especially O/I interfaces.

In the present work, we have carried out surface potential mapping by SKPM on ultrathin islands of the benchmark organic semiconductor pentacene grown on polymer dielectrics

Received: October 1, 2013
Revised: November 17, 2013
Published: January 27, 2014

ACS Publications © 2014 American Chemical Society

dx.doi.org/10.1021/jp409768j | J. Phys. Chem. C 2014, 118, 2487−2497

in order to quantify electronic polarization at different pentacene/dielectric interfaces (see Figure 1). The influence

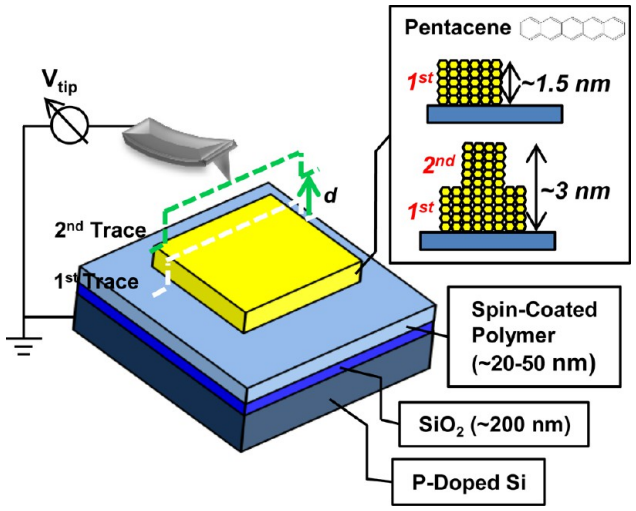

Figure 1. Schematic of surface potential mapping by SKPM of ultrathin (1−2 monolayers) pentacene films deposited on a variety of polymeric substrates. Pentacene was thermally deposited on polystyrene (PS), poly(methyl methacrylate) (PMMA), poly(α-methyl styrene) (PαMS), poly(4-vinyl phenol) (PVPh), along with *para*-substituted PS derivatives, including poly(4-methylstyrene) (PMS), poly(4-*tert*-butylstyrene) (P*t*BS), poly(4-bromostyrene) (PBS), and poly(4-chlorostyrene) (PCS). The polymer films were fabricated by spin-coating corresponding polymer solutions onto SiO_2/p++ silicon wafers. A conductive probe scans across the sample surface in a two-pass "lift mode" with a constant lift height of 10 nm and simultaneously records the topography and surface potential of the sample.

of polymer type and deposition conditions, i.e., the substrate temperature, on CPDs has been examined. There is good correlation between the CPD magnitudes and the dipole moments of the characteristic monomers of the polymer substrates. Furthermore, the surprising intralayer surface potential variations of the crystalline pentacene islands are correlated with microstructure. Specifically, we propose that intra-island surface potential domains reflect differences in epitaxial order. Overall, the visualization of electronic polarization through spatially resolved measurements of surface potentials and CPDs provides an effective approach to understanding fundamental electronic processes and electrostatic complexity at organic interfaces.

EXPERIMENTAL METHODS

Sample Preparation. All the pentacene films were prepared by thermal evaporation of the source material pentacene (Fluka, 99.8%) onto different dielectric polymer substrates with the chamber pressure $\leq 2 \times 10^{-6}$ torr and a deposition rate ~0.01 Å/s. A quartz crystal microbalance (QCM) was used to control the film coverage by targeting ~30−40% coverage for pentacene submonolayers and ~120−130% for pentacene two-layer films. The polymer substrates included polystyrene (PS), poly(methyl methacrylate) (PMMA), poly(α-methyl styrene) (PαMS), poly(4-vinyl phenol) (PVPh), and para-substituted PS, namely poly(4-methylstyrene) (PMS), poly(4-*tert*-butylstyrene) (P*t*BS), poly(4-bromostyrene) (PBS), and poly(4-chlorostyrene) (PCS). The properties of these polymers are summarized in the Supporting Information. All the substrates were prepared by spin coating corresponding polymer solutions (PMMA, PαMS: 10 wt % polymer/1,2-dichloroethane solution; PS, and PS derivatives: 5 wt % polymer/toluene solution; PVPh: 5 wt % polymer/ethanol solution) onto thermally grown SiO_2 (~200 nm) on p-doped silicon wafers (2000 rpm, 30 s) and baked at 90 °C for 1 h to remove residual solvent. According to atomic force microscopy (AFM) measurements, all the spin-coated polymer films have thicknesses around 20−50 nm. The substrate temperatures were varied from room temperature (27 °C) to 60 °C for different depositions.

Scanning Probe Microscopy. All the SPM measurements were performed with a Bruker Nanoscope V Multimode 8 Scanning Probe Microscope inside an argon-filled glovebox with oxygen level <5 ppm.

Scanning Kelvin Probe Microscopy. SKPM has been utilized to measure the surface potential of as-deposited pentacene films. To allow comparison between different cases, the same tip was used throughout all the measurements. SKPM is a noncontact SPM method capable of probing the local surface potential distributions while simultaneously mapping the topography. Commonly, it operates in a two-pass interleave mode or "lift mode". In the first pass, the specimen is scanned by a sharp conducting probe in regular attractive regime dynamic mode for topography. To stabilize performance in the attractive regime, the cantilever is driven at a drive frequency slightly larger than the fundamental resonant frequency, and the set point amplitude is about 90% of the free amplitude. In the second pass, the probe is lifted to a constant height above the surface, and the surface is scanned over again along the same topographic trajectory to preserve constant average distance between probe and sample. In the operational procedure of the second pass, the mechanical vibration of the cantilever is zeroed, and an ac voltage is applied to induce the vibration of the cantilever. The vibrational amplitude is nulled with a feedback circuit that adjusts an additional dc voltage bias of the tip (per surface location) to match that of the local surface; this local surface potential is directly recorded as the dc voltage. The attractive regime dynamic mode is preferred for our SKPM measurement (i.e., in the first pass that generates the topography image) since it better preserves the probe and thereby allows meaningful surface potential comparison among different films by eliminating probe-to-probe variation. Note that the same probe (tip/cantilever) was used for all the SKPM measurements shown here, but these results were representative of a large body of experiments using different probes. The typical probes were from Mikromasch USA (DPER 18, Pt coated, resonant frequency 60−90 kHz, spring constant 2.0−5.5 N/m, and tip radius 30 nm). The lift height during the second pass was 10 nm, which was beyond the range where van der Waals forces come into play. The applied ac voltage in SKPM was 0 to +6 V in amplitude.

Histogram Analysis. All histogram analyses were performed using freeware *Gwyddion*. To obtain well-defined surface potential distributions for different surface regions instead of one broad potential distribution for all the regions, individual regions were selectively masked using surface potential thresholding. (For those surface potential images with worse differentiation, masks were created via thresholding of the simultaneously obtained topography image and then applied to the surface potential images.) Histogram analysis was performed for the masked regions, and all extracted histograms for different surface regions were overlaid in graphs to compare

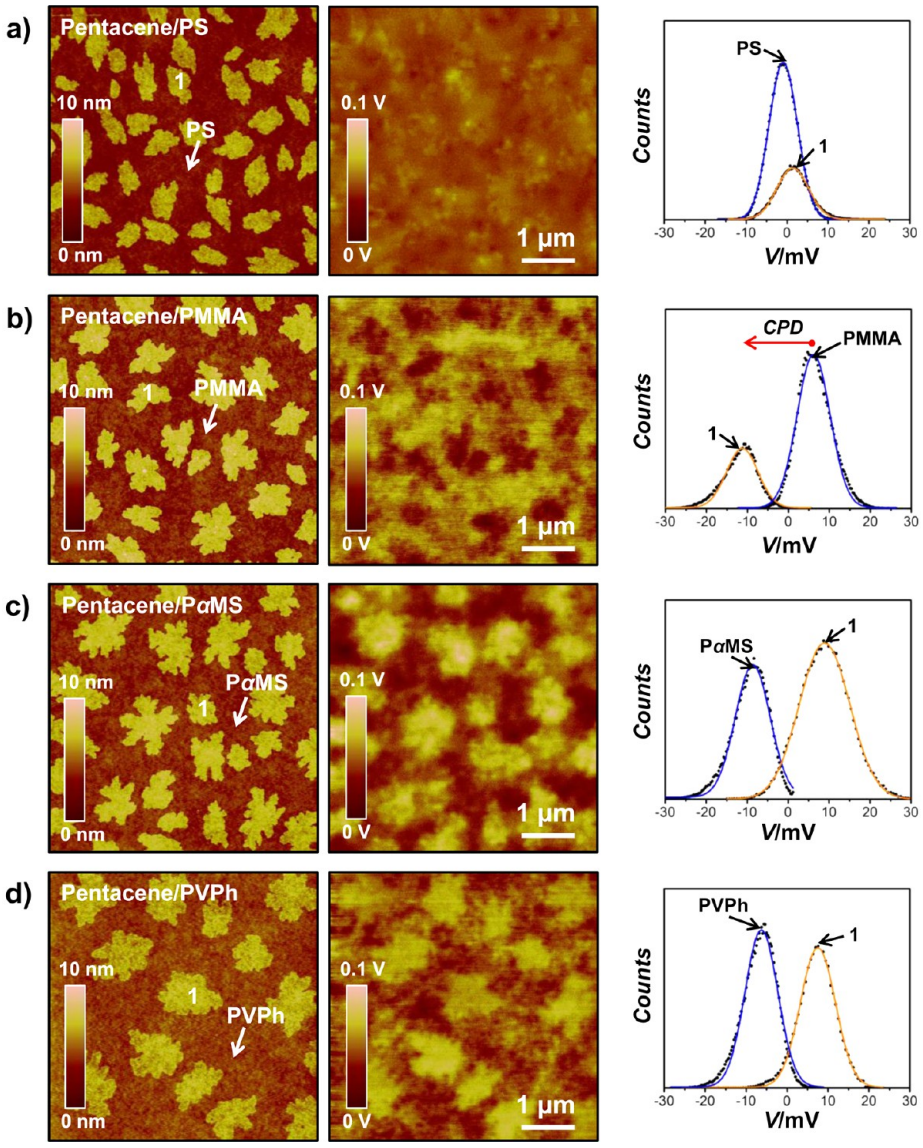

Figure 2. Topography, surface potential, and potential histogram of pentacene submonolayer islands grown on four common polymer dielectrics. (a) Topography, surface potential, and potential histogram of pentacene submonolayer deposited on PS. The bright islands in the topographic image represent pentacene grains. They exhibit very similar surface potential compared to PS as shown in the surface potential image. The potential histogram shows the potential distribution peaks of PS and pentacene which are <5 mV apart. (b) Topography, surface potential, and potential histogram of pentacene submonolayer grown on PMMA. The topography shows bright pentacene grains on dark substrate. Pentacene grains have more negative surface potential than PMMA. The CPD (∼−20 mV) is defined as the peak surface potential difference between that of pentacene and polymer and is the same for elsewhere. (c) Topography, surface potential, and potential histogram of pentacene submonolayer on P*α*MS. Bright pentacene islands and dark P*α*MS substrate are shown in the topographic image. The pentacene islands display more positive surface potential with respect to the substrate. Histogram analysis gives a CPD of ∼+20 mV. (d) Topography, surface potential, and potential histogram of pentacene submonolayer on PVPh with pentacene islands being brighter in both topography and surface potential image, meaning that pentacene grains have more positive surface potential than PVPh. According to the potential histogram, the CPD is ∼+15 mV.

the surface potential distributions within a given image. (A detailed example is provided in the Supporting Information.) An alternative method was to extract the histogram from an entire image and perform single- or multipeak Gaussian curve fits to distinguish the potential distributions from different regions. A comparison of the histograms obtained from the two methods is made in the Supporting Information. Importantly, it is meaningless to compare the absolute position of each peak among different histograms since a plane fit has been applied to the images that offsets the absolute peak position in order to bring the average of all peaks in a histogram to the zero-position.

Dipole Moment Calculation. ChemBio3D Ultra 13.0 integrated with ChemBioDraw Ultra 13.0 was used to compute dipole moments of the monomers for different polymers. The molecular structure of each monomer was built by ChemBioDraw and then displayed in 3D by ChemBio3D. The dipole moment of corresponding structure was then computed by the ab initio electronic structure calculation program GAMESS interface which is included in the software.

RESULTS AND DISCUSSION

Effect of Substrate Type on Contact Potential Difference. Crystalline pentacene islands were grown by

dx.doi.org/10.1021/jp409768j | J. Phys. Chem. C 2014, 118, 2487−2497

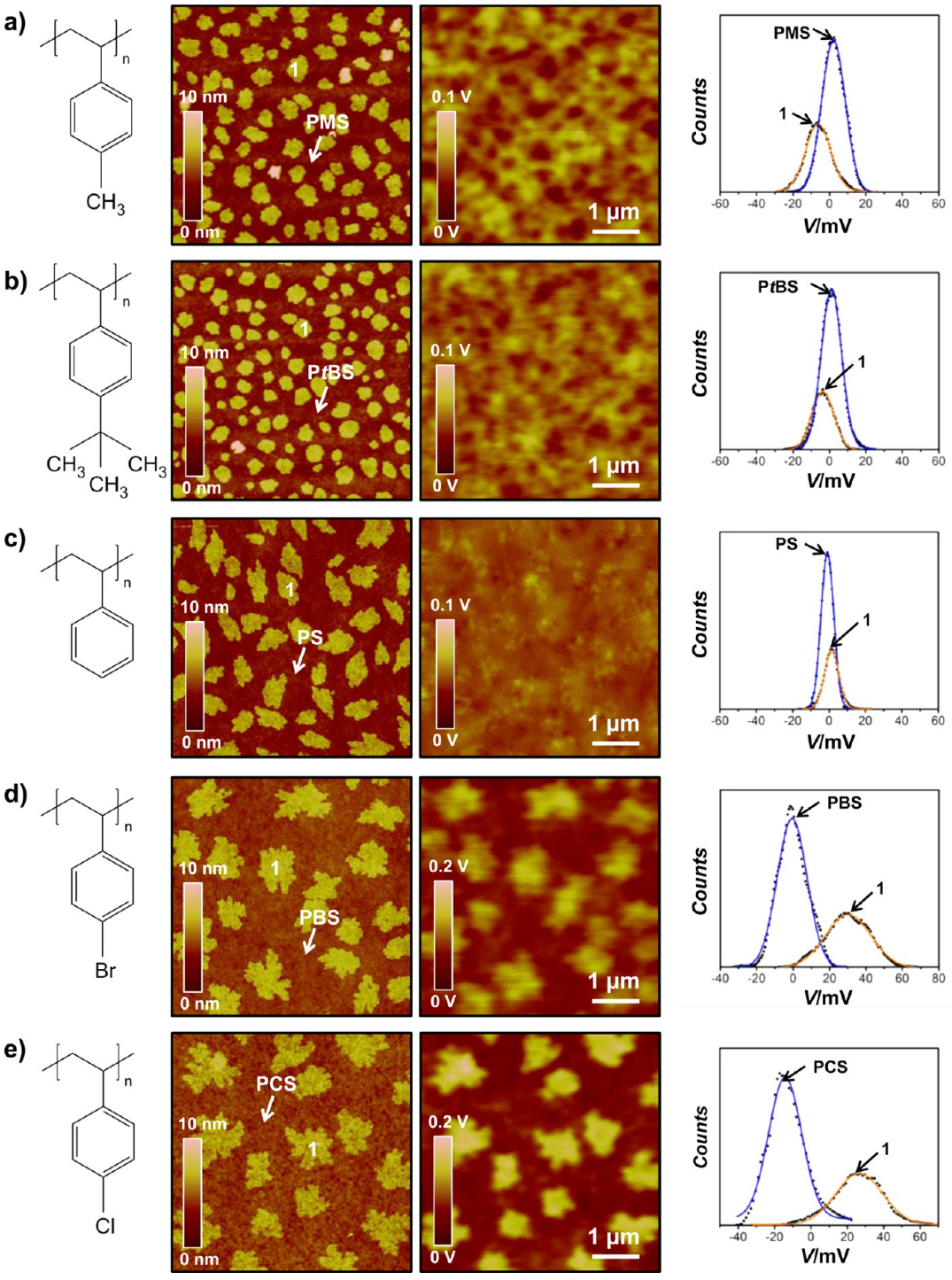

Figure 3. Topography, surface potential, and potential histogram of pentacene submonolayer islands grown on PS and *para*-substituted derivatives of PS. (a) Topography, surface potential, and potential histogram of submonolayer pentacene deposited on PMS. Pentacene islands exhibit more negative surface potential than PMS, and the CPD is ∼−10 mV. (b) Topography, surface potential, and potential histogram of submonolayer pentacene grown on P*t*BS. Pentacene grains have slightly more negative surface potential than P*t*BS, giving rise to a CPD of ∼−5 mV. (c) Topography, surface potential, and potential histogram of pentacene submonolayer on PS. The pentacene islands display very similar surface potential with respect to the substrate, and the CPD is <+5 mV. (d) Topography, surface potential, and potential histogram of pentacene submonolayer on PBS with pentacene islands showing more positive surface potential than PBS. The potential histogram shows a CPD of ∼+30 mV. (e) Topography, surface potential, and potential histogram of pentacene submonolayer PCS, and pentacene grains are more positive in surface potential than PCS. The CPD is ∼+40 mV according to the potential histogram.

thermal deposition in a vacuum chamber at 10^{-6} torr onto a variety of polymer films. Four common polymer dielectrics for OFETs, including PS, PMMA, PαMS, and PVPh, were selected as substrate materials. Notably, the convenience of spin coating relatively smooth surfaces with root-mean-square (rms) roughnesses below 0.5 nm over the lateral scale of interest (∼20 μm) facilitated the formation of dispersed micrometer-sized, monolayer thick pentacene islands.

dx.doi.org/10.1021/jp409768j | *J. Phys. Chem. C* 2014, 118, 2487−2497

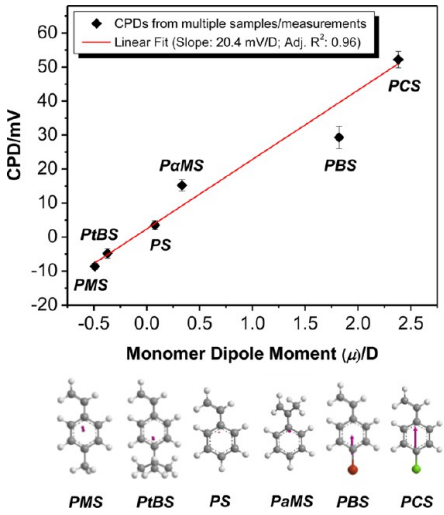

Figure 4. Quantitative summary of CPDs as a function of the monomer dipole moment. All the films were deposited when the substrates were at room temperature. The plotted CPDs were calculated using the surface potential peaks of pentacene and substrate, respectively, from potential histograms of at least two different samples in six measurements. The dipole moments of the monomers were calculated using the software *ChemDraw*. The CPD varies essentially linearly with the dipole moment of characteristic monomers.

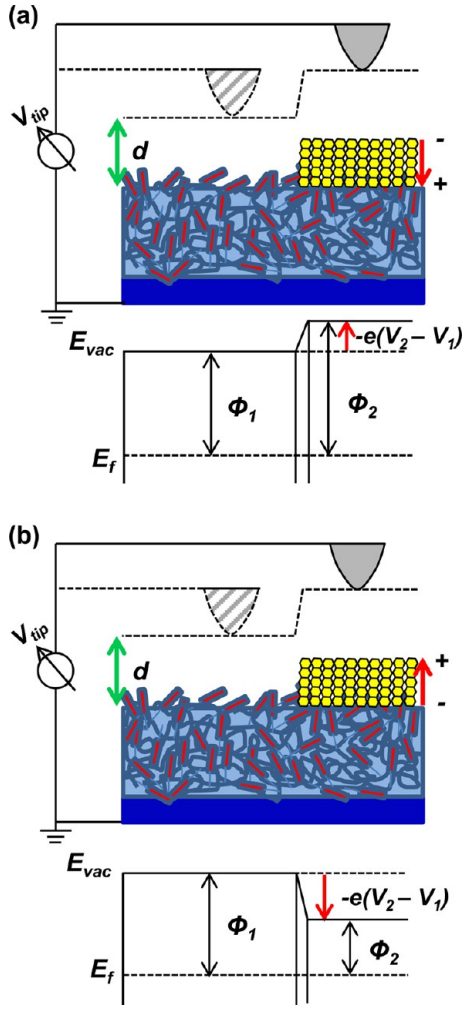

Figure 5. Energy level diagram illustration of the surface potential measurement. (a) Pentacene molecules are polarized in a way that the positive end of the dipole points into the surface, which leads to an upward shift of the vacuum level (E_{vac}). Additional negative bias thus has to be applied when the probe scans from bare polymer to the pentacene islands and it equals the CPD (CPD = $V_2 - V_1$), and darker pentacene grains on brighter substrate are shown in the surface potential map. A net dipole moment pointing into the polymer surface can be deduced. (b) Pentacene molecules are polarized with the positive end of the dipole pointing out of the surface, resulting in a downward vacuum level shift. When the probe scans from bare polymer to pentacene islands, additional positive bias equal to CPD (CPD = $V_2 - V_1$) is applied so that the surface potential map shows brighter pentacene grains on darker substrate. This implies that the polymer surface has net dipoles pointing out of the surface.

Figure 2 displays representative topography and corresponding surface potential images of monolayer pentacene islands grown on PS, PMMA, PαMS, and PVPh films. All substrates were kept at room temperature during film deposition. Very similar grain morphology was observed for all samples, characterized as dendritic to compact islands with measured heights corresponding to one standing pentacene molecule (~1.5 nm). It is well-known that pentacene molecules grown on inert substrate adopt a herringbone, edge-to-face packing motif and the molecules stand nearly vertically in each layer with the [001] direction being approximately perpendicular to the substrate.[32,33] Thus, there are no face-on molecules in all investigated pentacene submonolayers, and the darker (lower) regions in the topographic images correspond to bare polymer.

The surface potential images in Figure 2 show substantial differences for islands grown on different substrates. Note that all the surface potential measurements presented in this work were carried out using the same probe, which is necessary for meaningful comparisons. Moreover, surface potential of bare polymer films was measured prior to pentacene deposition, and no significant changes of tip−polymer CPDs were observed upon pentacene deposition. In the case of the PS substrate (Figure 2a), the surface potential of the pentacene islands is very close to that of PS. Thus, in this case, within the resolution of SKPM,[34−36] the pentacene grains are almost indistinguishable in the surface potential image. However, significant pentacene-to-substrate surface potential contrast exists in the three other samples. Pentacene displays more negative surface potential than PMMA (Figure 2b). Pentacene grains grown on PαMS (Figure 2c) and PVPh (Figure 2d), on the other hand, show more positive surface potential with respect to the substrates. Both the magnitude and sign of the surface potential contrast change with the polymer substrate type.

Quantitative analyses of the surface potential images are shown in the histograms in Figure 2. Instead of conventional histogram analysis which simply counts all data points in an image and typically generates a broad distribution, here independent histogram analyses were performed individually for pentacene islands and the substrates. This procedure diminishes the "edge effects", i.e., the capacitive convolution caused by the finite probe size.[34] That is, those data points located near island boundaries (as determined from the height images) were intentionally neglected during image analyses. Following this approach, two well-defined peak positions are evident in the potential histograms in Figure 2. We take the CPD to be the difference in surface potentials between the pentacene islands and the substrate, i.e., the CPD = $V_{pentacene} - V_{polymer}$, where $V_{pentacene}$ and $V_{polymer}$ are the peak surface potentials (approximately the mean surface potentials) in each

dx.doi.org/10.1021/jp409768j | J. Phys. Chem. C 2014, 118, 2487−2497

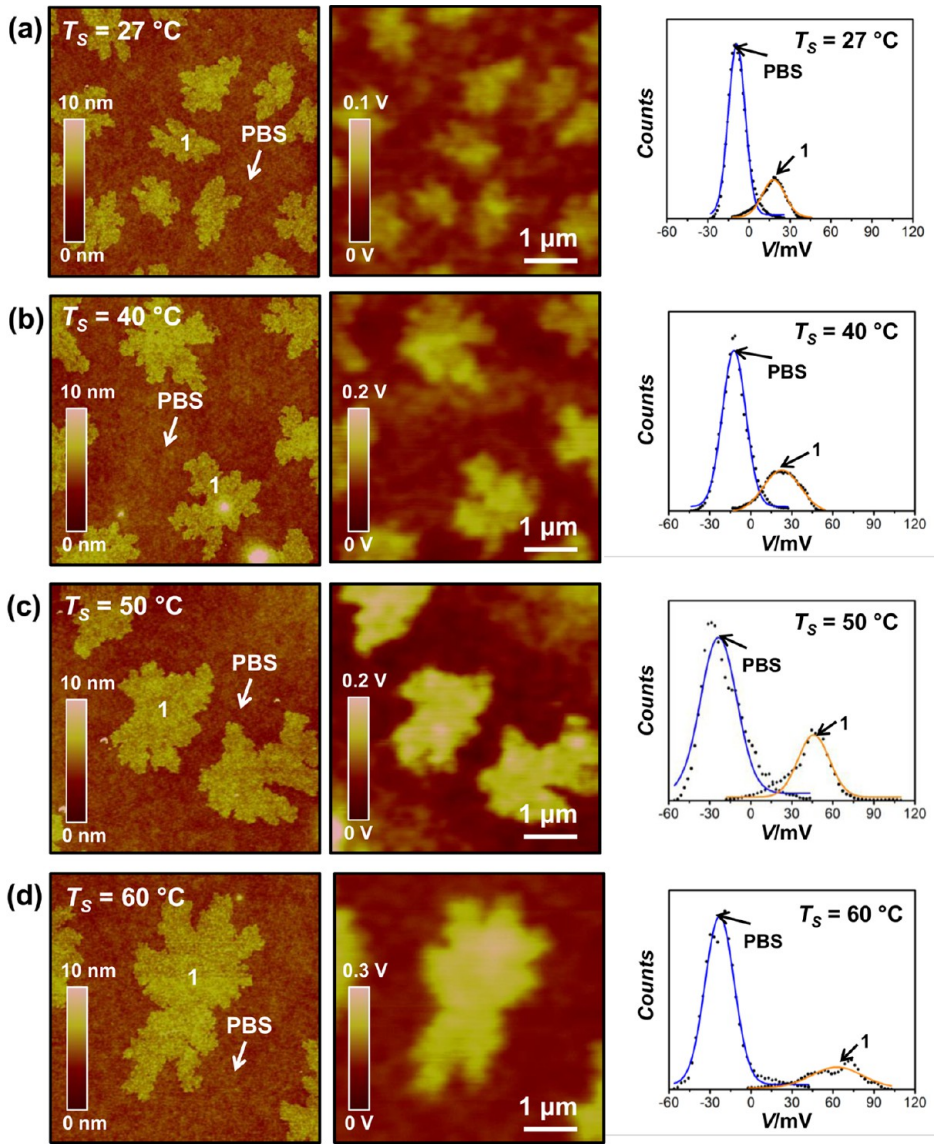

Figure 6. Topography, surface potential, and potential histogram of submonolayer pentacene grown on PBS at different substrate temperature (T_S). (a) Topography, surface potential, and potential histogram of pentacene submonolayer deposited at T_S = 27 °C. Pentacene islands displays more positive surface potential than the substrate, and the histogram analysis gives a CPD of ∼+30 mV. (b) Topography, surface potential, and potential histogram of pentacene submonolayer deposited at T_S = 40 °C. The pentacene grains show more positive surface potential than PBS, and the CPD is ∼+45 mV as seen in the histogram. (c) Topography, surface potential, and potential histogram of pentacene submonolayer deposited at T_S = 50 °C. The pentacene grains show more positive surface potential than PBS. The histogram gives a CPD of ∼+75 mV. (d) Topography, surface potential, and potential histogram of pentacene submonolayer deposited at T_S = 60 °C. Pentacene displays more negative surface potential than the substrate with the CPD being ∼+90 mV.

domain. The CPDs range from ∼+5 mV for pentacene/PS interfaces to ∼± 20 mV for the others. Again, it is interesting that both the sign and the magnitude of the CPDs depend on the polymer type.

To investigate the role of the polymer substrate more systematically, the same SKPM measurements were performed using a family of para-substituted PS polymers (PSX) as the substrates: PS, PMS, P*t*BS, PBS, and PCS. The monomers of these polymers have systematically varying permanent dipole moments (μ) that depend on the para-substituent, as calculated using the software *ChemDraw*: μ_{CS} (2.38 D) > μ_{BS} (1.82 D) > μ_S (0.08 D) > μ_{tBS} (−0.37 D) > μ_{MS} (−0.49 D). The topography and surface potential of submonolayer pentacene films grown on PS and the four types of para-substituted PS at room temperature are compared in Figure 3. Again, similar morphology was observed in all cases, but with the island shape slightly varying from more compact to more dendritic from Figure 3a to 3e. The surface potential and CPDs varied significantly across the sample set. Unlike pentacene/PS interfaces, all four other pentacene/PSX interfaces exhibited significant CPDs. Pentacene displayed slightly more negative surface potential (∼−10 mV) than PMS (Figure 3a) and P*t*BS (Figure 3b), whereas pentacene grown on PBS (Figure 3d) and PCS (Figure 3e) showed distinctively more positive surface potential than the substrates (∼+30−50 mV). The potential histograms clearly reveal the surface potential distributions of pentacene and the substrate. The peak separation reveals the different CPD values.

Figure 4 summarizes the CPD data. The CPDs between pentacene and the corresponding substrate are plotted using

dx.doi.org/10.1021/jp409768j | *J. Phys. Chem. C* 2014, 118, 2487−2497

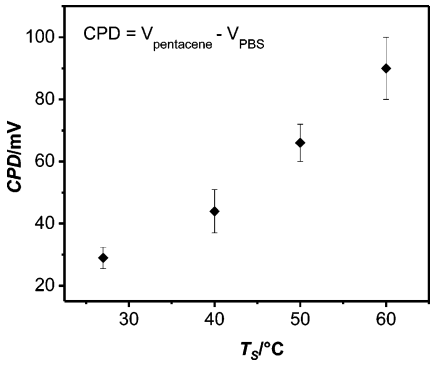

Figure 7. Quantitative summary of CPDs for samples deposited on PBS at different substrate temperature (T_S). The plotted CPD is defined as the surface potential difference between pentacene grains and PBS, and each CPD was obtained from the histograms of at least two different samples in six measurements. Significant increase of CPD can be seen with increasing T_S.

the histogram peak positions from six measurements of at least two different samples. The CPD data have been ordered according to the dipole moments of the substrate monomers which are shown on the *x*-axis of the plot. It is striking that the CPD between pentacene and the substrate can be as large as +50 mV in the case of pentacene/PCS interfaces. Also, it is clear that the CPD varies systematically, essentially linearly, with the dipole moment of the characteristic monomers. That is, the surface potential of pentacene islands relative to the substrate (or the CPD) is negative on alkyl-substituted PS, positive on halogen-substituted PS, and close to neutral on PS. The case of P*α*MS is interesting as the monomer has a significant dipole (~0.3 D) approximately perpendicular to the phenyl ring, yet the CPD still falls reasonably close to the trend line. Furthermore, pentacene/PMS and P*t*BS interfaces exhibit smaller CPD magnitudes than pentacene/PBS and PCS interfaces, consistent with the fact that the dipole moments (relative magnitudes) of MS (~0.49 D) and *t*BS (~0.37 D) are much smaller than that of BS (~1.82 D) and CS (~2.38 D).

The probable origin of the polarization in the pentacene/polymer systems is induced polarization of pentacene molecules, not charge transfer. This could be attributed to static dipoles associated with the polymer surface or so-called cooperative dipoles formed by specific noncovalent interactions between polymer chains and the pentacene molecules. Pentacene is known to have large inherent polarizability along its long axis due to the 22 anisotropically delocalized π-electrons in its backbone.[37] We imagine that pentacene molecules in contact with PCS, for example, could be polarized by the strong dipole moment of the CS monomer. There may also be noncovalent interactions between pentacene and the substituent Cl.[38] Either effect, or both, could then induce a dipole in pentacene. Overall, it is clear that the interfacial polarization we observe is directly related to the nature of the polymer substrate.

It should be noted that the linear relationship in Figure 4 should be viewed as approximate and applicable to the homologous series of PS polymers we have investigated. The dipole moments have been calculated for the monomers using *ChemDraw*, and we have verified their approximate correctness where possible by comparison to the literature values.[39,40] Furthermore, as shown in the Supporting Information (Figure S7), CPD data for PMMA and PVPh do not fall on the trend line. The behavior of these more hydrophilic substrates (see water contact angle data in the Supporting Information, Table S1) appears to be different than the behavior of the PS series polymers. Nevertheless, the overall trend in Figure 4 suggests a good correlation between the monomer dipole of the PS polymers and the CPD. We have also carefully excluded other possible contributions to the systematic CPD results, such as the dielectric constant and glass transition temperature of the polymers. Further investigations of other effects including polymer polarizability would also be interesting, but we view them as less likely contributors to the CPD trend.

Energy level diagrams are also helpful to further interpret the surface potential and CPD results. According to the above results, films with distinctive CPDs between pentacene and substrate fall into two categories with pentacene islands being either more negative or more positive than the substrate. The energy level diagrams for these two cases are illustrated in Figures 5a and 5b, respectively.

A more negative surface potential atop the pentacene islands compared to the bare polymer (e.g., PMS and P*t*BS) suggests an energy band diagram as shown in Figure 5a. The regions covered by pentacene islands have a smaller CPD relative to the SKPM tip (more negative surface potential) than the bare polymer so that the alignment of Fermi level results in an upward shift of the vacuum level (E_{vac}) from bare polymer to pentacene-covered polymer. The induced dipole must have its positive end pointing into the surface, which is possible when there are net static dipoles at the polymer surface (due to the MS and *t*BS monomers) that are oriented in the same direction. In contrast, for PBS and PCS samples, the pentacene islands are positive, i.e., they have a larger CPD relative to the SKPM tip, and thus the vacuum level shifts downward over pentacene, Figure 5b. This then implies that dipoles with their positive ends point out of the surface. As mentioned above, the origin of the interface dipoles could be static dipoles associated with oriented monomers at the polymer surface, or it is possible that a noncovalent bond forms between the halogen atom in the polymer and the hydrogen atom in pentacene.[38] Either mechanism could shift the π-electrons in pentacene such that the positive end of the induced dipole is pointing out of the surface.

Effect of Growth Temperature on Contact Potential Difference. The impact of deposition conditions on the surface potential has also been examined. Specifically, the substrate temperature during pentacene deposition was systematically varied, and the surface potential of as-deposited films was measured by SKPM. Figure 6 shows one example of isolated pentacene islands deposited on PBS. Since the desorption of pentacene becomes more favorable or even dominant when the substrate temperature exceeds 70 °C, the substrate temperature study was constrained within the temperature range of room temperature (27 °C) to 60 °C with an increment of about 10 °C. Clearly, the substrate temperature strongly impacts the grain size and nucleation density as demonstrated in the topographic images. The films tend to have larger grains but smaller nucleation densities with elevated substrate temperature owing to thermally facilitated diffusion of pentacene molecules at higher substrate temperature.[33,41,42] Importantly, the substrate temperature significantly impacts the surface potential of the films as illustrated in the images and the potential histograms in Figure 6. As the substrate temperature increases, the pentacene surface potential shifts positively.

dx.doi.org/10.1021/jp409768j | J. Phys. Chem. C 2014, 118, 2487−2497

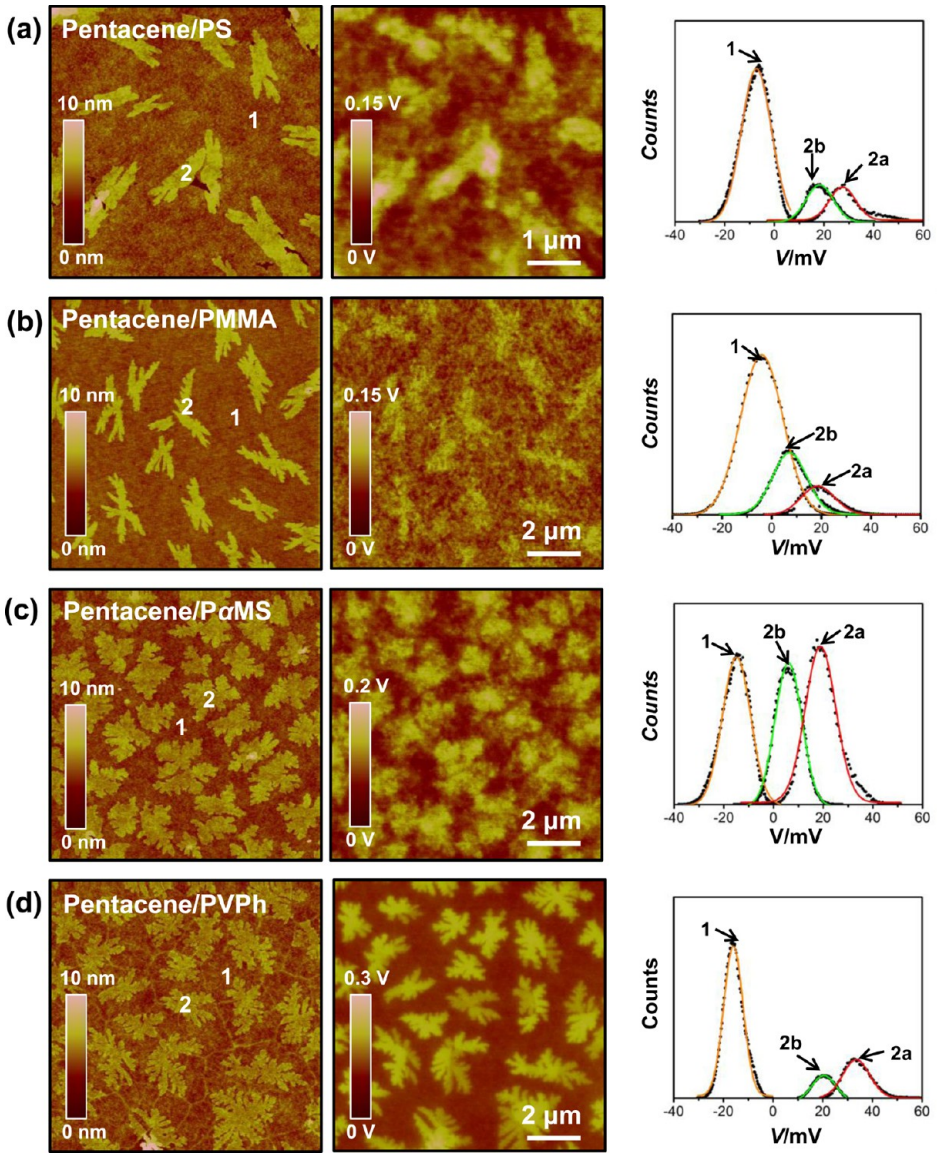

Figure 8. Topography, surface potential, and potential histogram of pentacene two-layer films grown on four common polymer dielectrics. (a) Topography, surface potential, and potential histogram of pentacene film deposited on PS with low coverage of second layer. Pentacene second layer islands exhibit more positive surface potential than the first layer. A potential histogram also gives two distinct domains within the second layer (red and green curves in histogram). (b) Topography, surface potential, and potential histogram of pentacene two-layer film deposited on PMMA with some second layer grains nucleating on top of fully closed first layer. Pentacene second layer shows more positive surface potential than the first layer, but the difference is less than 10 mV. The potential histogram also shows two distinct potential domains of the second layer. (c) Topography, surface potential, and potential histogram of pentacene film grown on PαMS with complete first layer and some second layer grains. Pentacene second layer grains show more positive surface potential than the first layer. The potential histogram also shows two distinct potential domains of the second layer. (d) Topography, surface potential, and potential histogram of pentacene deposited on PVPh with some second layer grains and fully closed first layer. Pentacene second layer shows more positive surface potential than the first layer, and there are two distinct potential domains within the second layer.

Figure 7 shows the extracted CPDs versus growth temperature. There is an overall positive increase ranging from ∼+30 mV at room temperature to ∼+90 mV at 60 °C. The causes of this CPD increase with growth temperature may include structural changes in either the pentacene or polymer layers, or thermally induced strain in pentacene, for example. It is important that the effect is significant, i.e., there is a +60 mV increase in CPD upon changing the deposition temperature from room temperature to 60 °C, but the precise cause of this effect will require further investigation. Similar substrate temperature studies were carried out for pentacene grains deposited on other substrates (see the Supporting Information). For all cases the CPDs consistently exhibited sensitivity to the growth substrate temperature, although the trends with temperature varied.

Microstructure and Surface Potential Domains. Pentacene exhibits Stranski–Krastanov (wetting layer plus island) growth behavior[41] on all polymer substrates investigated here. SKPM was employed to record surface potentials in the second layer islands which grow on a completely closed monolayer. Figure 8 shows the result for ∼3 nm thick pentacene films deposited on the four common polymer substrates (i.e., PS, PMMA, PαMS, and PVPh) at room temperature. All films exhibit similar morphology with dendritic

dx.doi.org/10.1021/jp409768j | J. Phys. Chem. C 2014, 118, 2487−2497

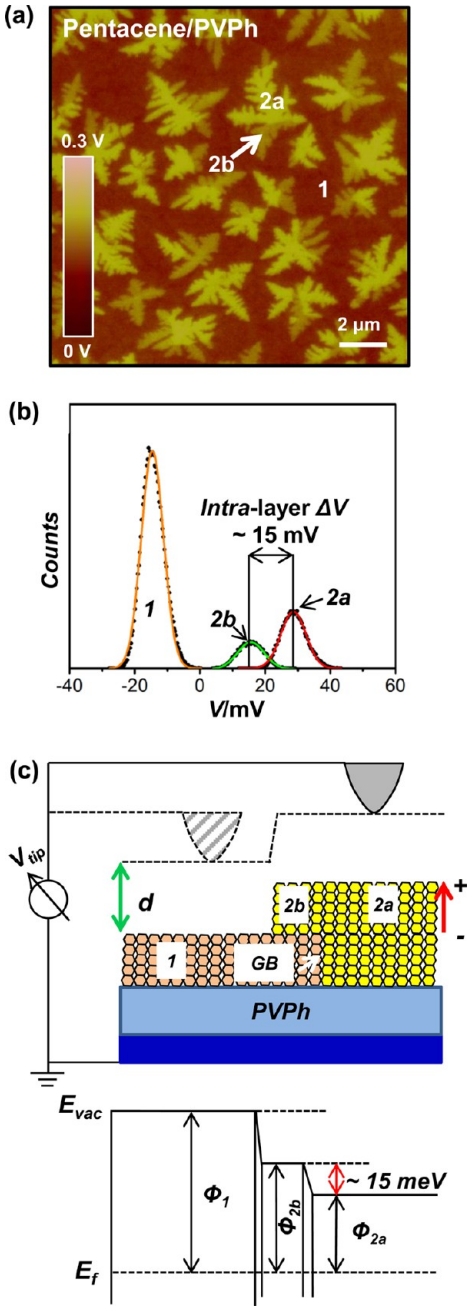

Figure 9. (a) Surface potential of pentacene two-layer film on PVPh with fully coalesced first monolayer and a few dendritic second islands. There are two different surface potential domains within the second layers, indicated as 2a (more positive surface potential) and 2b (less positive surface potential) domains. (b) Histogram shows surface potential variations of pentacene film shown in (a). Surface potential difference (ΔV) between 2a and 2b domains (red and green curves) is ~15 mV. (c) Energy level diagram illustration of the surface potential measurement of the film in (a). Pentacene second layer molecules are polarized with the positive end of the dipole pointing out of the surface, leading to a downward vacuum level shift. For the 2a domain, which is epitaxial relative to its underlayer, the vacuum level shift is ~15 meV more downward than the 2b domain which overgrows to a different first layer grain.

second layer grains growing on top of a fully closed first layer. It is immediately evident from Figure 8 that the surface potentials of the second layer islands, although they vary with the substrates in magnitude, are always positive relative to the closed first layer. This is true even for the film grown on the PMMA substrate, which exhibited a negative CPD for the first monolayer (see Figure 2). Positive surface potentials are expected in the case of pentacene grown on PαMS and PVPh, because in those cases the first pentacene monolayer had a positive CPD and one could anticipate that polarization in the underlying pentacene first layer should induce a similar polarization in the second layer. The origin of positive surface potential for second layer islands on PMMA, on the other hand, might be structural changes (e.g., crystalline order) in the second layer relative to the first. Surface potentials (work functions) are known to be very sensitive to crystal structure and defect densities.[43−45] We will return to this point below.

Closer inspection of the images in Figure 8 reveals that the intralayer potential landscapes are more complex in the second layer than for the first layer. Specifically, there are two potential domains, 2a and 2b, in the second layer islands. This is particularly evident for the PαMS and PVPh substrates, Figures 8c and 8d, respectively, where the difference in potential between 2a and 2b domains is extraordinarily clear.

Figure 9a shows the surface potential image of pentacene films grown on PVPh with 2a and 2b domains unambiguously resolved. The potential histogram (Figure 9b) clearly illustrates that the intralayer surface potential difference is ~15 mV. According to the potential histograms in Figure 8, this difference is indeed independent of the substrate type, in contrast to the aforementioned interlayer surface potential contrast which shows a strong substrate dependence. More importantly, the intralayer surface potential difference is also independent of the deposition condition, i.e., substrate temperature (see the Supporting Information), which is again different from the interlayer surface potential difference.

Such intralayer surface potential variation has also been observed in our previous studies in pentacene films grown on SiO_2.[46,47] We have proposed that the potential domains 2a and 2b result from differences in homoepitaxy, i.e., that 2a is an epitaxial domain and 2b is nonepitaxial.[47] We have based this on friction force microscopy (FFM) results that consistently show that the 2a domain has lower friction (is more ordered) than the 2b domain.[47] Similar friction/surface potential relationships were observed in pentacene/polymer films examined here (see the Supporting Information). Determining whether the potential and friction domains are really different epitaxial domains will require further investigation, which is ongoing in our laboratory. However, the possible correlation of crystalline order with surface potential (work function) is certainly intriguing. For example, a correlation between more positive surface potential (lower work function) and order may mean that second layer islands are uniformly more ordered (fewer defects) on all substrates, as these islands always have more positive surface potentials. Figure 9c shows an energy level diagram illustrating these concepts, where the crystalline epitaxial regions (yellow-on-yellow) have the smallest work function. More generally, the possible use of surface potential mapping to identify domains of more or less order would be extremely useful for understanding microstructure of crystalline soft materials. More work on probing the generality of the result is ongoing in our laboratory. For the purposes of this paper, it is important to note that our new results here show that the 2a and 2b potential domains occur regardless of the substrate type, i.e., whether the substrate is SiO_2 or a variety of different polymer films.

dx.doi.org/10.1021/jp409768j | J. Phys. Chem. C 2014, 118, 2487−2497

CONCLUSION

We have carried out quantitative SKPM measurements on ultrathin pentacene films (1−3 nm) thermally deposited on different polymer dielectrics. Systematic investigation of monolayer thick pentacene islands on polymers reveals that the CPDs of the pentacene/polymer interfaces strongly depend on the substrate type and deposition condition, i.e., substrate temperature. Furthermore, SKPM of two-layer thick pentacene films grown on different substrates shows that the surface potential of the second layer pentacene islands is always positive relative to the underlying first monolayer, probably owing to a more ordered structure in the second layer. Intralayer surface potential differences have been consistently observed in all pentacene films and are believed to arise from microstructure/epitaxial variations. Our investigations reveal important factors that influence the interfacial electronic properties in a benchmark O/I interface and also raise important open questions of how microstructure (e.g., homoepitaxy) affects electronic properties in soft, polarizable organic semiconductor materials. In closing, it is worthwhile noting that surface potential (work function) variations will result in band-edge fluctuations, which in turn imply a disordered landscape for charge carriers at O/I interfaces.

ASSOCIATED CONTENT

Supporting Information

Summary of polymer properties; details of histogram analysis and comparison with conventional method; effect of substrate temperature on contact potential difference for pentacene on different polymer substrates; CPDs as a function of monomer dipole moment for all investigated polymers; effect of substrate temperature on intralayer potential difference; correlation between friction and surface potential for pentacene deposited on PS, PMMA, PαMS, and PVPh. This material is available free of charge via the Internet at http://pubs.acs.org.

AUTHOR INFORMATION

Corresponding Author

*E-mail: frisbie@umn.edu.

Notes

The authors declare no competing financial interest.

ACKNOWLEDGMENTS

This work was primarily supported by the National Science Foundation under Grant No. DMR-0706011 and was partially supported by the MRSEC Program of the National Science Foundation under Grant No. DMR-0819885. Parts of this work were carried out in the Characterization Facility, University of Minnesota, which received partial support from NSF through the MRSEC program.

REFERENCES

(1) Braun, S.; Salaneck, W. R.; Fahlman, M. Energy-Level Alignment at Organic/Metal and Organic/Organic Interfaces. *Adv. Mater.* **2009**, *21*, 1450−1472.

(2) Cahen, D.; Kahn, A. Electron Energetics at Surfaces and Interfaces: Concepts and Experiments. *Adv. Mater.* **2003**, *15*, 271−277.

(3) Fukagawa, H.; Yamane, H.; Kera, S.; Okudaira, K.; Ueno, N. Experimental Estimation of the Electric Dipole Moment and Polarizability of Titanyl Phthalocyanine Using Ultraviolet Photoelectron Spectroscopy. *Phys. Rev. B: Condens. Matter Mater. Phys.* **2006**, *73*, 041302.

(4) Gao, Y. Surface Analytical Studies of Interfaces in Organic Semiconductor Devices. *Mater. Sci. Eng. R.* **2010**, *68*, 39−87.

(5) Ishii, H.; Sugiyama, K.; Ito, E.; Seki, K. Energy Level Alignment and Interfacial Electronic Structures at Organic/Metal and Organic/Organic Interfaces. *Adv. Mater.* **1999**, *11*, 605−625.

(6) Hwang, J.; Wan, A.; Kahn, A. Energetics of Metal−Organic Interfaces: New Experiments and Assessment of the Field. *Mater. Sci. Eng. R* **2009**, *64*, 1−31.

(7) Schlaf, R.; Parkinson, B. A.; Lee, P. A.; Nebesny, K. W.; Armstrong, N. R. Determination of Frontier Orbital Alignment and Band Bending at an Organic Semiconductor Heterointerface by Combined X-ray and Ultraviolet Photoemission Measurements. *Appl. Phys. Lett.* **1998**, *73*, 1026−1028.

(8) Koch, N. Electronic Structure of Interfaces with Conjugated Organic Materials. *Phys. Status Solidi RRL* **2012**, *6*, 277−293.

(9) Zhu, X.; Kahn, A. Electronic Structure and Dynamics at Organic Donor/Acceptor Interfaces. *MRS Bull.* **2010**, *35*, 443−448.

(10) Crispin, X.; Geskin, V.; Crispin, A.; Cornil, J.; Lazzaroni, R.; Salaneck, W. R.; Brédas, J.-L. Characterization of the Interface Dipole at Organic/ Metal Interfaces. *J. Am. Chem. Soc.* **2002**, *124*, 8131−41.

(11) Monti, O. L. A.; Steele, M. Influence of Electrostatic Fields on Molecular Electronic Structure: Insights for Interfacial Charge Transfer. *Phys. Chem. Chem. Phys.* **2010**, *12*, 12390−400.

(12) Wang, S.; Sakurai, T.; Kuroda, R.; Akimoto, K. Energy Band Bending Induced Charge Accumulation at Fullerene/Bathocuproine Heterojunction Interface. *Appl. Phys. Lett.* **2012**, *100*, 243301.

(13) Brabec, C. J.; Sariciftci, N. S.; Hummelen, J. C. Plastic Solar Cells. *Adv. Funct. Mater.* **2001**, *11*, 15−26.

(14) Wilke, A.; Endres, J.; Hörmann, U.; Niederhausen, J.; Schlesinger, R.; Frisch, J.; Amsalem, P.; Wagner, J.; Gruber, M.; Opitz, A.; et al. Correlation between Interface Energetics and Open Circuit Voltage in Organic Photovoltaic Cells. *Appl. Phys. Lett.* **2012**, *101*, 233301.

(15) Logdlund, M.; Salaneck, W. R.; Lögdlund, M. Conjugated Polymer Surfaces and Interfaces in Polymer-Based Light-Emitting Diodes. *Polym. Adv. Technol.* **1998**, *9*, 419−428.

(16) Parthasarathy, G.; Adachi, C.; Burrows, P. E.; Forrest, S. R. High-Efficiency Transparent Organic Light-Emitting Devices. *Appl. Phys. Lett.* **2000**, *76*, 2128−2130.

(17) Malenfant, P. R. L.; Dimitrakopoulos, C. D. Organic Thin Film Transistors for Large Area Electronics. *Adv. Mater.* **2002**, *14*, 99−117.

(18) Chabinyc, M.; Lujan, R.; Endicott, F.; Toney, M.; McCulloch, I.; Heeney, M. Effects of the Surface Roughness of Plastic-Compatible Inorganic Dielectrics on Polymeric Thin Film Transistors. *Appl. Phys. Lett.* **2007**, *90*, 233508.

(19) Zhang, H.; Guo, X.; Hui, J.; Hu, S.; Xu, W.; Zhu, D. Interface Engineering of Semiconductor/Dielectric Heterojunctions Toward Functional Organic Thin-Film Transistors. *Nano Lett.* **2011**, *11*, 4939−46.

(20) Yang, S. Y.; Shin, K.; Park, C. E. The Effect of Gate-Dielectric Surface Energy on Pentacene Morphology and Organic Field-Effect Transistor Characteristics. *Adv. Funct. Mater.* **2005**, *15*, 1806−1814.

(21) Veres, J.; Ogier, S.; Lloyd, G.; de Leeuw, D. Gate Insulators in Organic Field-Effect Transistors. *Chem. Mater.* **2004**, *16*, 4543−4555.

(22) Salleo, A.; Chabinyc, M. L.; Yang, M. S.; Street, R. A. Polymer Thin-Film Transistors with Chemically Modified Dielectric Interfaces. *Appl. Phys. Lett.* **2002**, *81*, 4383−4385.

(23) Koch, N. Organic Electronic Devices and Their Functional Interfaces. *Chem. Phys. Chem.* **2007**, *8*, 1438−55.

(24) Chen, L.; Ludeke, R.; Cui, X.; Schrott, A.; Kagan, C.; Brus, L. Electrostatic Field and Partial Fermi Level Pinning at the Pentacene−SiO_2 Interface. *J. Phys. Chem. B* **2005**, *109*, 1834−8.

(25) Fujihira, M. Kelvin Probe Force Microscopy of Molecular Surfaces. *Annu. Rev. Mater. Sci.* **1999**, *29*, 353−380.

(26) Ikeda, S.; Shimada, T.; Kiguchi, M.; Saiki, K. Visualization of Induced Charge in an Organic Thin-Film Transistor by Cross-Sectional Potential Mapping. *J. Appl. Phys.* **2007**, *101*, 094509.

(27) Luo, Y.; Gustavo, F.; Henry, J.-Y.; Mathevet, F.; Lefloch, F.; Grévin, B.; Sanquer, M.; Rannou, P.; Grévin, B. Probing Local

Electronic Transport at the Organic Single-Crystal/Dielectric Interface. *Adv. Mater.* **2007**, *19*, 2267−2273.
(28) Palermo, V.; Palma, M.; Samori, P.; Palermo, M.; Palma, P. Electronic Characterization of Organic Thin Films by Kelvin Probe Force Microscopy. *Adv. Mater.* **2006**, *18*, 145−164.
(29) Pingree, L. S. C.; Rodovsky, D.; Coffey, D.; Bartholomew, G.; Ginger, D. S. Scanning Kelvin Probe Imaging of the Potential Profiles in Fixed and Dynamic Planar LECs. *J. Am. Chem. Soc.* **2007**, *129*, 15903−10.
(30) Puntambekar, K.; Pesavento, P.; Frisbie, C. D. Surface Potential Profiling and Contact Resistance Measurements on Operating Pentacene Thin-Film Transistors by Kelvin Probe Force Microscopy. *Appl. Phys. Lett.* **2003**, *83*, 5539−5541.
(31) Nonnenmacher, M.; O'Boyle, M. P.; Wickramasinghe, H. K. Kelvin Probe Force Microscopy. *Appl. Phys. Lett.* **1991**, *58*, 2921−2923.
(32) Fritz, S. E.; Martin, S. M.; Frisbie, C. D.; Ward, M. D.; Toney, M. F. Structural Characterization of a Pentacene Monolayer on an Amorphous SiO_2 Substrate with Grazing Incidence X-Ray Diffraction. *J. Am. Chem. Soc.* **2004**, *126*, 4084−5.
(33) Ribic, P. R.; Kalihari, V.; Frisbie, C. D.; Bratina, G. Growth of Ultrathin Pentacene Films on Polymeric Substrates. *Phys. Rev. B: Condens. Matter Mater. Phys.* **2009**, *80*, 115307.
(34) Jacobs, H. O.; Leuchtmann, P.; Homan, O.; Stemmer, A. Resolution and Contrast in Kelvin Probe Force Microscopy. *J. Appl. Phys.* **1998**, *84*, 1168−1173.
(35) Krok, F.; Sajewicz, K.; Konior, J.; Goryl, M.; Piatkowski, P.; Szymonski, M. Lateral Resolution and Potential Sensitivity in Kelvin Probe Force Microscopy: Towards Understanding of the Sub-Nanometer Resolution. *Phys. Rev. B: Condens. Matter Mater. Phys.* **2008**, *77*, 235427.
(36) Zerweck, U.; Loppacher, C.; Otto, T.; Grafström, S.; Eng, L. M. Accuracy and Resolution Limits of Kelvin Probe Force Microscopy. *Phys. Rev. B: Condens. Matter Mater. Phys.* **2005**, *71*, 125424.
(37) Tsiper, E. V.; Soos, Z. G. Electronic Polarization in Pentacene Crystals and Thin Films. *Phys. Rev. B: Condens. Matter Mater. Phys.* **2003**, *68*, 085301.
(38) Bryantsev, V. S.; Hay, B. P.; Are, C-H Groups Significant Hydrogen Bonding Sites in Anion Receptors? Benzene Complexes with Cl−, NO_3−, and ClO_4−. *J. Am. Chem. Soc.* **2005**, *127*, 8282−3.
(39) Parker, H.; Lombadi, J. R. Dipole Moment of the First Excited $\pi^*\leftarrow\pi$ States of Styrene. *J. Chem. Phys.* **1971**, *54*, 5095−5096.
(40) Chen, H. B.; Chang, T. C.; Chui, Y. S.; Ho, S. Y. Photopolymerization of Styrene, *p*-Chlorostyrene, Methyl Methacrylate, and Butyl Methacrylate with Poly(methylphenylsilane) as Photoinitiato. *J. Polym. Sci., Part A: Polym. Chem.* **1996**, *34*, 679−685.
(41) Ruiz, R.; Choudhary, D.; Nickel, B.; Toccoli, T.; Chang, K.-C.; Mayer, A. C.; Clancy, P.; Blakely, J. M.; Headrick, R. L.; Iannotta, S.; et al. Pentacene Thin Film Growth. *Chem. Mater.* **2004**, *16*, 4497−4508.
(42) Pratontep, S.; Brinkmann, M.; Nuesch, F.; Zuppiroli, L. Nucleation and Growth of Ultrathin Pentacene Films on Silicon Dioxide: Effect of Deposition Rate and Substrate Temperature. *Synth. Met.* **2004**, *146*, 387−391.
(43) Duhm, S.; Heimel, G.; Salzmann, I.; Glowatzki, H.; Johnson, R. L.; Vollmer, A. A.; Rabe, J.; Koch, N. Orientation-Dependent Ionization Energies and Interface Dipoles in Ordered Molecular Assemblies. *Nat. Mater.* **2008**, *7*, 326−32.
(44) Kajimoto, N.; Manaka, T.; Iwamoto, M. Decay Process of a Large Surface Potential of Alq_3 Films by Heating. *J. Appl. Phys.* **2006**, *100*, 053707.
(45) Suchko, P. V.; Shluger, A. L.; Catlow, R. A. Relative Energies of Surface and Defect States: Ab Initio Calculations for the MgO(001) Surface. *Surf. Sci.* **2000**, *450*, 153−170.
(46) Puntambekar, K.; Dong, J.; Haugstad, G.; Frisbie, C. D. Structural and Electrostatic Complexity at a Pentacene/Insulator Interface. *Adv. Funct. Mater.* **2006**, *16*, 879−884.
(47) Kalihari, V.; Ellison, D. J.; Haugstad, G.; Frisbie, C. D. Observation of Unusual Homoepitaxy in Ultrathin Pentacene Films and Correlation with Surface Electrostatic Potential. *Adv. Mater.* **2009**, *21*, 3092−3098.